

Lattice instabilities of $\text{PbZrO}_3/\text{PbTiO}_3$ [1:1] superlattices from first principles

Claudia Bungaro and K. M. Rabe

Department of Physics and Astronomy, Rutgers University, Piscataway, NJ 08854-8019

(March 15, 2022)

Ab initio phonon calculations for the nonpolar reference structures of the (001), (110), and (111) $\text{PbZrO}_3/\text{PbTiO}_3$ [1:1] superlattices are presented. The unstable polar modes in the tetragonal (001) and (110) structures are confined in either the Ti- or the Zr-centered layers and display two-mode behavior, while in the cubic (111) case one-mode behavior is observed. Instabilities with pure oxygen character are observed in all three structures. The implications for the ferroelectric behavior and related properties are discussed.

I. INTRODUCTION

The soft-mode theory of ferroelectrics¹ has established the relationship of the unstable polar modes of a high-symmetry nonpolar reference structure to the physics of both the ferroelectric transition and the large dielectric and piezoelectric coefficients. First-principles density functional perturbation theory (DFPT),^{2,3} permits the direct quantitative investigation of such unstable modes and the accurate computation of the interatomic force constants, phonon frequencies and dynamical matrix eigenvectors of the cubic reference structures of ferroelectric perovskite oxides such as BaTiO_3 , PbTiO_3 , SrTiO_3 , and KNbO_3 , has lead to a deeper understanding of the individual compounds and materials trends⁴⁻⁷.

For technological applications requiring high-performance dielectrics, piezoelectrics, and ferroelectrics, the most promising candidates are not pure perovskite compounds, but solid solutions, such as $\text{Pb}(\text{Zr}_x\text{Ti}_{1-x})\text{O}_3$ (PZT)⁸, $(\text{Ba}_x\text{Sr}_{1-x})\text{TiO}_3$ (BST)⁹ and PMN-PT¹⁰, and atomic-scale superlattices including $\text{BaTiO}_3/\text{SrTiO}_3$ and $\text{KNbO}_3/\text{KTaO}_3$.¹¹ In these systems, the unstable polar modes of their high-symmetry nonpolar reference structure are similarly expected to be central to a predictive understanding of their properties. However, their chemical and structural complexity, requiring the use of large supercells, leads to a tremendous increase in the computational demands of first-principles calculations.

Accurate first-principles calculations can be performed only for short period superlattices and the simplest ordered configurations of solid solutions. PZT is a natural choice for first-principles investigation. Not only is it already in widespread use in piezoelectric transducer applications, but its optimal composition, at the morphotropic phase boundary, is almost exactly $x=0.5$, which corre-

sponds to ordered structures with supercells as small as double the primitive perovskite unit cell. Indeed, work on the (001) and (111) doubled supercells dominates available first-principles results on PZT.¹²⁻¹⁶ While the atomic arrangements in real bulk PZT are of course much more disordered, the study of the lattice dynamics of ordered structures with [1:1] compositional modulation along various crystallographic directions provides (i) an accurate characterization of the phonons of ultrathin superlattices, (ii) a guide to understanding the vibrational properties of the disordered alloys, and (iii) a quantitative benchmark to develop and test ab initio based approximations that can accurately describe the lattice dynamics of disordered solid solutions and large scale heterostructures, and are computationally more amenable than direct first-principles calculations.

In this paper, we present first-principles calculations for the lattice dynamics of three ordered configurations of $\text{Pb}(\text{Zr}_{0.5}\text{Ti}_{0.5})\text{O}_3$: the [1:1] ultrathin superlattices (001), (110) and (111). In Section II, we give the details of the computations. In Section III, we present the relaxed nonpolar structures, phonon dispersions along selected directions, and detailed analysis of the unstable modes. Several interesting features not present in the pure end-point compounds, and the implications for the ferroelectric behavior and related properties, are identified and discussed in Section IV.

II. COMPUTATIONAL METHOD

We performed ab initio calculations using density functional theory (DFT) with the plane wave pseudopotential method. The vibrational properties were computed using density functional perturbation theory (DFPT)¹⁷ generalized to ultrasoft pseudopotentials.¹⁸ All calculations were performed using the PWSCF and PHONON codes.¹⁹

We used Vanderbilt ultrasoft pseudopotentials²⁰, treating as valence states the $3s$, $3p$, $3d$, and $4s$ electrons of Ti, the $4s$, $4p$, $4d$, and $5s$ electrons of Zr, the $5d$, $6s$, and $6p$ electrons of Pb, and the $2s$ and $2p$ electrons of O. The inclusion of the semi-core electrons in the valence states is necessary for an accurate description of these oxides. The exchange and correlation energy is given within the local density approximation (LDA) using the parameterization of Perdew and Zunger²¹. A kinetic energy cut-off of 35 Ry was used and the augmentation charges were expanded up to 350 Ry. For PZT(001), (110) and (111), the Brillouin zone (BZ) integration was performed

using 12 (663 tetragonal mesh), 9 (446 tetragonal mesh) and 6 (333 fcc mesh) \mathbf{k} -points in the irreducible BZ, respectively.

For the prototypical cubic perovskite structure of the pure materials, PbZrO_3 (PZ) and PbTiO_3 (PT), we obtained the following values for the theoretical equilibrium lattice parameter: $a(\text{PZ})=7.77$ a.u. and $a(\text{PT})=7.37$ a.u. (experimental values 7.81 a.u. and 7.50 a.u.) and bulk modulus $B(\text{PZ})=170$ GPa and $B(\text{PT})=202$ GPa. These compare very well with results from previous LDA calculations, such as Ref. 22.

To compute the LO-TO splitting at Γ arising from the long-range Coulomb interactions present in the perovskite oxides, it is necessary to know the electronic dielectric tensor ϵ_∞ and the Born effective charge tensors \mathbf{Z}_s^* , where s runs over the atoms in the unit cell. These can be computed within the framework of DFPT, although the current version of PHONON allows these computations only with norm-conserving pseudopotentials. For the calculation of ϵ_∞ and \mathbf{Z}_s^* we have therefore used Troullier and Martins pseudopotentials²³ with the same valence states as for the ultrasoft pseudopotentials. To achieve convergence with the norm-conserving pseudopotentials an energy cutoff of 80 Ry was needed. All the other parameters, such as lattice parameters, atomic positions, and \mathbf{k} -point sampling were chosen to be the same as those optimized with the ultrasoft pseudopotentials.

III. RESULTS

The primary focus of our calculations is the eigenfrequencies and eigenvectors of the unstable polar modes at Γ . The unstable eigenvectors of the analytic part of the dynamical matrix are of particular interest, since they generate symmetry-breaking energy-lowering distortions of the relaxed structures under conditions of zero macroscopic electric field. Some direct connections between features of the superlattice structure and the unstable modes emerge. In general, we will see that if pure Ti-O chains are present in the ordered structure, the lowest frequency unstable modes are confined in the PT layer and are characterized by displacements parallel to these chains. Another connection is between modes of the superlattice structures and those of strained bulk PT and PZ. This is especially easy to see in the ideal structure, where the relevant strain is an isotropic expansion for PT and compression for PZ. For the noncubic (001) and (110) structures, the LO-TO splitting gives rise to a nontrivial anisotropy with changing direction of the vanishing \mathbf{q} vector. Surprisingly, unstable LO modes are also found to occur. Throughout this section, symmetry analysis will be used to organize and present the results.

A. Relaxed structures

To find an appropriate high-symmetry reference structure for PZT, we first placed the atoms as in the ideal cubic perovskite structure with lattice constant $a(\text{PZT})=7.57$ a.u., obtained by averaging the theoretical values in the pure endpoint compounds PZ and PT. This value is very close to the LDA value of 7.55 a.u. calculated for PZT(111) by Fornari and Singh.¹⁶ The Zr and Ti atoms are ordered on the B sites to establish the (001), (110) and (111) [1:1] superlattices. These superlattice structures will be referred to below as “ideal” PZT(001), PZT(110) and PZT(111). The “relaxed” superlattice structures are then obtained by allowing symmetry preserving relaxations of the internal atomic coordinates, holding the lattice parameters fixed. The three ordered supercells each contain ten atoms, with the Wyckoff labels and corresponding atomic positions indicating the free internal structural parameters given in Table I.

The unit cell of PZT(001) is tetragonal, obtained by doubling the cubic perovskite cell along the [001] direction (space group D_{4h}^1). The lattice parameters are fixed at $a=a(\text{PZT})$ and $c=2a$. Alternating TiO_2 and ZrO_2 planes are separated by PbO planes along the [001] direction, the oxygens in the Wyckoff positions 2f, 2e, and 2g being coplanar with the Ti, Zr and Pb atoms, respectively. Pure Ti-O and Zr-O chains run along the [100] and [010] directions, perpendicular to the direction of compositional modulation, [001]. The symmetry preserving relaxation of the internal atomic coordinates consists of displacements along z of the atoms in the PbO planes (Pb and O(2g) atoms). In the ideal perovskite structure, the z values for Pb and O(2g) are exactly $z_{\text{Pb}} = z_{\text{O}} = 0.25$. After relaxation we find that the PbO planes shift almost rigidly towards the TiO_2 plane with $\Delta z_{\text{Pb}} = -0.20$ a.u. and $\Delta z_{\text{O}} = -0.19$ a.u., resulting in a lowering of the energy by 291 meV per unit cell. The relaxed Ti-O(2g) (Zr-O(2g)) distance is smaller (larger) than the corresponding distance in the pure compound PT (PZ). Since the BO_6 octahedron can be regarded as the building block of the perovskite structure, it is useful to compare the distortion of the TiO_6 and ZrO_6 octahedra in the supercell relative to the pure endpoint compounds. In the relaxed (001) structure the TiO_6 (ZrO_6) octahedron is stretched (compressed) in the (001) plane, due to the larger (smaller) lattice parameter ($a(\text{PT}) < a(\text{PZT}) < a(\text{PZ})$), and shrinks (expands) along the [001] direction of compositional modulation. This relaxation relieves some of the superlattice epitaxial strain by restoring the local volumes towards their equilibrium values in the bulk endpoint compounds, though the local c/a ratio is significantly changed.

The PZT(110) structure is also tetragonal (space group D_{4h}^1) with lattice parameters $a=\sqrt{2}a(\text{PZT})$ and $c=a(\text{PZT})$. Along the [001] direction, TiZrO_4 planes alternate with Pb_2O_2 . Within the TiZrO_4 planes the Ti and Zr atoms are placed in a 2D checkerboard arrange-

ment, each surrounded by four coplanar oxygen atoms in the 4j position. Pure Ti-O and Zr-O chains run along the [001] direction, perpendicular to the two equivalent directions of compositional modulation, [110] and $[1\bar{1}0]$. The symmetry preserving relaxation is specified by a single parameter Δx , the displacement of the four O(4j) atoms along the Ti-Zr lines in the TiZrO_4 planes. In the ideal perovskite structure the O atoms are exactly halfway between Ti and Zr, with $x=0.25$. After relaxation we find $\Delta x = -0.125$ a.u., so that the four coplanar O(4j) atoms surrounding the Ti (Zr) are 0.025 a.u. closer (further) than in PT (PZ), resulting in a lowering of the energy by 338 meV per unit cell. Compared to the pure endpoint compounds the TiO_6 (ZrO_6) octahedron is stretched (compressed) along the [001] direction, and shrinks (expands) in the (001) plane of compositional modulation. As in PZT(001), this relaxation relieves some of the superlattice epitaxial strain by restoring the local volumes towards their equilibrium values in the bulk endpoint compounds, though the local c/a ratio is significantly changed.

The PZT(111) structure is obtained by placing Ti and Zr atoms on the simple cubic lattice of B sites in the 3D checkerboard arrangement corresponding to the rocksalt structure (space group O_h^1). The unit cell is face centered cubic with lattice parameter $a=2a(\text{PZT})$. There are no pure Ti-O or Zr-O chains in this structure; in all B-O chains the Ti and Zr alternate. The symmetry-preserving relaxation is specified by a single parameter, Δx , corresponding to a breathing of the oxygen octahedra around the Ti and Zr atoms. A negative value of Δx corresponds to a breathing-in (breathing-out) motion around the Ti (Zr) atoms. In the ideal perovskite structure, the O atoms are exactly halfway between Ti and Zr, with $x = 0.25$. After relaxation we find that the oxygen atoms have moved closer to the Ti, with $\Delta x = -0.115$ a.u., resulting in a lowering of the energy by 465 meV per unit cell. The superlattice TiO_6 and ZrO_6 oxygen octahedra are remarkably similar to those in the pure endpoint compounds. Thus, at least with respect to the BO_6 octahedra (the Pb atoms are fixed), the superlattice strain is completely relaxed.

B. \mathbf{Z}^* and ϵ_∞

The computed electronic dielectric tensor ϵ_∞ and the Born effective charge tensors \mathbf{Z}_s^* for the relaxed PZT(001) and PZT(110) structures are given in Tables II and III. All matrices are diagonal except for $\mathbf{Z}_{O(4j)}^*$ in PZT (110) (note that in PZT(110) the xy axes are rotated by 45 degrees around z with respect to the original cubic axes), and therefore, except in that case, only the diagonal elements are given.

The anisotropy associated with the atomic ordering is generally quite small. Also, while \mathbf{Z}_{Zr}^* and \mathbf{Z}_{Ti}^* are quite different in the endpoint compounds, even when

computed at the same lattice constant $a(\text{PZT})$, the effective charges of Zr and Ti in the superlattices are very similar.¹⁴ As a result, the dielectric tensor and effective charges obtained by averaging the tensors for pure PT and pure PZ, also given in Tables II and III, are very close to the corresponding quantities for the superlattices. In fact, the change in LO phonon frequencies obtained by using the average values of ϵ_∞ and \mathbf{Z}_s^* instead of the superlattice values is in each case less than 2%, comparable to the overall accuracy expected for the first-principles calculation. The average values might therefore be expected to be a good approximation in other $x=0.5$ structures as well. The results that follow were computed using the average values.

C. Phonon dispersion

For the three relaxed (001), (110), and (111) PZT superlattices, the phonon dispersion along the direction of compositional modulation and the anisotropy at $q = 0$ are shown in Figure 1. In this section, we give an overview of the results, with detailed discussion and analysis to follow in Sections IIID, E and F.

The behavior of the phonon dispersion along the direction of compositional modulation indicates the degree to which the phonon vibrations are confined to layers of a particular composition. This dispersion is quite flat for most of the modes in the (110) and, to an even greater degree, in the (001) superlattices. This means that the corresponding normal modes are strongly localized within atomic planes perpendicular to the direction of compositional modulation. In contrast, most of the modes in the (111) superlattice display significant dispersion, indicating that the normal mode amplitudes are spread through the supercell. This will be confirmed by the analysis of individual eigenmodes below.

Due to the long-range character of the Coulomb force, the dynamical matrix displays non-analytic behaviour in the limit $\mathbf{q} \rightarrow 0$, resulting in a dependence of the frequencies and eigenvectors on the direction of the vanishing wave vector, $\hat{\mathbf{q}}$. More precisely, in the long wavelength limit the dynamical matrix can be written as the sum of an analytic contribution, $\mathbf{D}^T(q=0)$, and a non-analytic contribution that depends on the Born effective charge tensors \mathbf{Z}_s^* and the electronic dielectric tensor ϵ_∞ :

$$\mathbf{D}_{ss'}(\mathbf{q} \rightarrow 0) = \mathbf{D}_{ss'}^T(q=0) + \frac{4\pi e^2}{\Omega \sqrt{M_s M_{s'}}} \frac{(\mathbf{Z}_s^* \cdot \hat{\mathbf{q}})(\hat{\mathbf{q}} \cdot \mathbf{Z}_{s'}^*)}{\hat{\mathbf{q}} \cdot \epsilon_\infty \cdot \hat{\mathbf{q}}}, \quad (1)$$

where $\mathbf{D}^T(q=0)$ is the dynamical matrix computed with the boundary condition of zero macroscopic electric field ($\mathbf{E}=0$), M_s is the atomic mass of the atom s , and Ω is the volume of the unit cell.^{24,25} In the lefthand panels of the three plots in Figure 1, we show how the frequencies depend on the angle θ between the direction of the vanishing wave vector, $\hat{\mathbf{q}}$, and the direction of compositional

modulation. For a cubic structure, such as the (111) superlattice, the limiting frequencies do not depend upon the angle θ and can simply be identified as LO (longitudinal optic) and TO (transverse optic), though as in the perovskite structure, with multiple optic modes of the same symmetry, no one-to-one correspondence can be made between individual TO and LO modes²⁶. For the tetragonal (001) and (110) superlattices, the limiting frequencies do depend on the angle θ . This gives rise to bands of LO frequencies which can be identified by their dispersion in Figure 1 and which will be discussed in detail in Section III F.

All three superlattices display lattice instabilities; in fact, their phonon spectra contain entire branches of imaginary frequencies. The imaginary frequencies are indicated by the negative values in Figure 1 and the corresponding region of unstable modes is shaded in gray. The most unstable mode is observed at Γ in all three cases, consistent with our expectation that as for bulk PZT, the ground state of these superlattices should be ferroelectric. However, (111) is anomalous in that this dominant Γ mode is actually a nonpolar pure oxygen mode that will not produce a ferroelectric ground state, as will be discussed in more detail below. In the following, we focus on the behavior at the zone center, with particular attention to the unstable modes.

D. Unstable eigenmodes of $D^T(q=0)$

Diagonalization of the analytic contribution to the dynamical matrix, $D^T(q=0)$, gives the energies of the normal modes in zero macroscopic field. These modes can be classified using the full symmetry of the point group of the space group, as will be described in detail below. The transverse IR-active phonons (TO) and the non-polar phonons are eigenmodes of $D^T(q=0)$ as well as of the full dynamical matrix, while the LO modes are mixed by the nonanalytic contribution, as will be seen in Section F.

Since $D^T(q=0)$ has the full symmetry of the point group of the space group, we can classify its eigenmodes according to the irreducible representations (irreps) of D_{4h} for PZT(001) and PZT(110) and O_h for PZT(111), following the nomenclature of Ref. 27. These labels specify the polar character of the modes, which atoms are involved in the vibration, and the directions of the corresponding atomic displacements.

For the (001) superlattice, the eigenmodes are labelled by five irreps:

$$8\Gamma_{5'}^{(2)} \oplus 2\Gamma_5^{(2)} \oplus 6\Gamma_{1'} \oplus 2\Gamma_1 \oplus 2\Gamma_{3'}.$$

where the coefficient gives the multiplicity of the irrep and the superscript indicates its dimension. The two-dimensional irreps $\Gamma_{5'}$ and Γ_5 correspond to vibration in the xy-plane perpendicular to the direction of compositional modulation (\perp). The others are one-dimensional

irreps and correspond to vibrations along the direction of compositional modulation (\parallel). There are twelve IR-active polar TO modes (seven $\Gamma_{5'}(\perp)$ and five $\Gamma_{1'}(\parallel)$ modes) in which all of the atoms participate. The remaining $\Gamma_{5'}$ mode and $\Gamma_{1'}$ mode are the zero-frequency acoustic modes. All the other modes are non-polar: the two $\Gamma_{3'}$ modes involve only O(2e) and O(2f) z-vibrations, the two Γ_1 modes involve only O(2g) and Pb z-vibrations, and the two Γ_5 modes involve only O(2g) and Pb xy-vibrations.

For the (110) superlattice, the eigenmodes are labelled by nine irreps:

$$8\Gamma_{5'}^{(2)} \oplus \Gamma_5^{(2)} \oplus 6\Gamma_{1'} \oplus \Gamma_{3'} \oplus \Gamma_{4'} \oplus \Gamma_1 \oplus \Gamma_2 \oplus \Gamma_3 \oplus \Gamma_4.$$

These irreps correspond to vibrations in the xy-plane of compositional modulation (\parallel) or to vibrations in the perpendicular z direction (\perp). As in the (001) supercell there are twelve IR-active polar TO modes (seven $\Gamma_{5'}(\parallel)$ and five $\Gamma_{1'}(\perp)$) in which all of the atoms participate. The remaining $\Gamma_{5'}$ mode and $\Gamma_{1'}$ mode are the zero-frequency acoustic modes. All the other modes are non-polar: the $\Gamma_{3'}$ mode involve only Pb z-vibrations, the $\Gamma_{4'}$ and Γ_5 modes involve only O(4j) z-vibrations, and the Γ_1 , Γ_2 , Γ_3 , Γ_4 modes also involve only O(4j) vibrations but in the xy plane.

For the (111) supercell the eigenmodes are labelled by nine irreps:

$$5\Gamma_{15}^{(3)} \oplus 2\Gamma_{25'}^{(3)} \oplus \Gamma_{25}^{(3)} \oplus \Gamma_{15'}^{(3)} \oplus \Gamma_{12}^{(2)} \oplus \Gamma_1.$$

There are four IR-active polar TO modes, Γ_{15} , which involve atomic displacements of all the atoms along x, y or z. The remaining Γ_{15} mode is the acoustic zero frequency mode. All the other modes are non-polar: the two $\Gamma_{25'}$ modes are the odd linear combination of the two Pb(x,y,z) and one oxygen displacement pattern, and the remaining Γ_{25} , $\Gamma_{15'}$, Γ_{12} , and Γ_1 are all unique pure oxygen modes.

For both the ideal and relaxed structures of the three superlattices, the eigenfrequencies and symmetry labels of the *unstable* eigenmodes of $D^T(q=0)$ are given in Table IV. A comparison of the instabilities of the three ideal superlattice structures provides information on their sensitivity to the atomic configuration. In the ideal structures the atomic positions are identical and the only difference is in the arrangement of Zr and Ti atoms on the B sites. It can immediately be seen that the unstable eigenfrequencies are quite sensitive to the arrangement of atoms on the B site. In part, this reflects the different displacement patterns imposed by symmetry. Even if the Zr and Ti atoms were completely equivalent, these lists would differ because of the different q-points of the primitive Brillouin zone that are folded into the smaller cubic Brillouin zone of each supercell (Γ and X for (001), Γ and R for (111), and Γ and M for (110)), so only half of the modes (those from primitive Γ) would match for each pair. With the actual atoms in place the mixing

of the different “folded” mode combinations gives quite different results in the three superlattices.

For each superlattice structure, the effect of atomic relaxation has been investigated by comparing frequencies of the ideal structure with those of the relaxed structure. In PZT(001) the shift in frequencies is substantial, and in some cases even leads to a reordering of the modes (for example, the unstable $\Gamma_{3'}$ and $\Gamma_{5'}$ modes). The relaxations in the other two superlattice structures cause smaller changes. The larger shift in PZT(001) may be due to the larger atomic relaxations observed in this structure, which involve Pb displacements in addition to the oxygen displacements.

The unstable polar TO modes will be described in detail in the next section. In addition, each of the three superlattice structures has one pure oxygen instability. The oxygen instability in PZT(001), the $\Gamma_{3'}$ mode, is mainly confined in the PZ layers and corresponds to the Γ_{25} mode of bulk PZ. In the superlattice the PZ layers are under compressive strain ($a(\text{PZT}) < a(\text{PZ})$) and the origin of this oxygen instability is in the pressure dependence of the Γ_{25} mode of PZ which becomes unstable under compression. We note that this $\Gamma_{3'}$ oxygen instability is very sensitive to strain. In fact, the atomic relaxation alone causes a large shift of its eigenfrequency. The oxygen instability in PZT(110), the Γ_2 mode, is a rotation of the oxygen octahedra around the [001] direction and corresponds to an M mode of the primitive bulk cubic cell. In PZT(111) the oxygen instability is the most unstable Γ_{25} mode. It involves the rotation of the oxygen octahedra around the $\langle 111 \rangle$ directions and corresponds to the bulk R_{25} mode. This unstable mode contributes to the orthorhombic antiferroelectric ground state of pure PZ and is responsible for the tetragonal antiferrodistortive ground state of SrTiO_3 . Comparing the instabilities of PZT(111) with those of PZT(001) and PZT(110), we see that the frequency of the oxygen instability is similar in all three systems. However, in PZT(111) the most unstable polar mode has been significantly shifted upwards, which we attribute to the lack of intact Ti-O chains in any direction. This leaves the oxygen instability as the dominant unstable mode.

E. Confined TO polar instabilities

Each of the three superlattice structures possesses TO polar instabilities, indicated in boldfaced type in Table IV, that can generate candidate ferroelectric structures. PZT(001) and PZT(110) exhibit “two-mode behavior,” that is, there are two types of such unstable modes, one with atomic displacements mainly confined in the PT layer and the other in the PZ layer. The atomic displacements of the two most unstable TO modes of relaxed PZT (001), $\Gamma_{5'}$ and $\Gamma_{1'}$, are shown in Figure 2. The $\Gamma_{5'}$ is a PT-like mode polarized parallel to the interfaces; it is confined in the PT layer and is remarkably

similar to the unstable TO mode of bulk PT (also shown in Figure 2 for comparison). The $\Gamma_{1'}$ mode, on the other hand, is a PZ-like mode polarized perpendicular to the interfaces; it is mainly confined in the PZ layer and is remarkably similar to the unstable TO mode in bulk PZ. The confinement of these modes in the PT and PZ layers is consistent with their flat dispersion for \mathbf{q} perpendicular to the interfaces.

The atomic arrangements and projections in the (110) and (111) structures do not lend themselves well to representation in a figure analogous to Figure 2. A convenient way of characterizing the confinement of the polar instabilities in all three superlattice structures is to decompose the mode effective charge, \bar{Z} , into two contributions: one from the Zr-centered cell and one from the Ti-centered cell: $\bar{Z} = \bar{Z}_{\text{Zr}} + \bar{Z}_{\text{Ti}}$. These local contributions to the mode effective charge, which will be referred to as “local effective charges,” are defined as

$$\bar{Z}_{\text{Ti(Zr)}} = \sum_{s,\beta} w_s Z_{\alpha\beta;s}^* u_{\beta,s} \quad (2)$$

where the sum over the atoms, s , runs only over the atoms in the Ti (Zr) centered cell and the weighting factor w_s is $w=1$ for Ti (Zr), $w=0.5$ for the 6 oxygen atoms and $w=0.125$ for the 8 Pb atoms. In the case that the modes are confined, we expect the local effective charge to have its largest value in the corresponding layer.

The local effective charges for PZT(001) have been included in Figure 2. For the PT-like mode, $\Gamma_{5'}$, $\bar{Z}_{\text{Ti}}=7.29$ is more than three times larger than \bar{Z}_{Zr} , indicating a high degree of confinement. Moreover, it is very close to the mode effective charge of the unstable TO mode in PT (at the equilibrium lattice constant), $\bar{Z}=7.57$, confirming the local similarity to the bulk PT unstable mode. For the PZ-like mode, $\Gamma_{1'}$, the larger contribution is from the Zr-centered cell, $\bar{Z}_{\text{Zr}}=4.93$, which is likewise very close to the mode effective charge of the unstable TO mode in PZ, $\bar{Z}=4.86$.

The local effective charges of the unstable TO modes of all three superlattice structures are given in Table V. By symmetry, the induced polarizations are parallel to the direction of atomic displacement for each mode, also included in the table. For almost every unstable TO mode of the (001) and (110) superlattices, either \bar{Z}_{Ti} or \bar{Z}_{Zr} strongly dominates, indicating that the polar instabilities are mainly confined either to the PT or to the PZ layers, respectively. The confined character of the modes is seen to be rather insensitive to the relaxation. Just as for the (001) case discussed above, the most unstable mode for PZT(110) is a PT-like mode with polarization aligned in the PT plane (perpendicular to the direction of compositional modulation, \perp) followed by a PZ-like mode with polarization parallel to the direction of compositional modulation, \parallel .

In contrast to the two-mode behavior of PZT(001) and PZT(110), PZT(111) exhibits one-mode behavior. For its single unstable TO mode, the local effective charges are

almost identical and the polar instability is distributed throughout the supercell. The different behavior of PZT (111) is a consequence of the fcc symmetry; in fact, the displacements of the six oxygens in the supercell are symmetry-related, so that any mode in which oxygen displacements are allowed will in general involve the whole supercell, preventing the confinement to occur.

There are two distinct factors that could produce the observed mode confinement: the difference between the atomic mass of the two species occupying the B sites (Ti and Zr) or the dependence of the interatomic force constants upon atomic configuration (i.e. the atomic force constants may depend upon the chemical identity of either of the two interacting atoms and upon the surrounding atomic configuration). In some semiconductor heterostructures, such as AlAs/GaAs^{28,29}, the interatomic force constants (IFCs) are to a good approximation unaffected by the substitution, Al/As, and the observed character of the heterostructure modes is the result of the difference in mass. One might hope that the isoelectronic substitution Ti/Zr could be similarly understood. To check this, the eigenfrequencies and local effective charges of the dynamical matrices in which the masses of Ti and Zr have been replaced by their average are shown in Table VI. Changing the value of the masses results in a frequency shift that is larger for those modes that involve larger displacements of the Ti or Zr ions. In particular the PT-like modes of (001) and (110) are shifted to higher frequency. The PZ-like modes are almost unaffected since the atomic displacements of Zr and Ti are almost zero in these modes. By the analysis of the local effective charges in Table VI it is evident that the mode confinement is still present when Ti and Zr have the same mass. It must therefore be that the IFCs depend strongly upon atomic configuration, with interactions involving Zr atoms significantly differing from their Ti counterparts. The important consequence of this observation is that approximations for the IFCs that neglect the effect of compositional modulation, with the most widely used being the virtual crystal approximation, cannot adequately capture the character of the instabilities in PZT.

F. LO-TO splitting and anisotropy at $q=0$

The effect of adding the non-analytic term to the dynamical matrix is to mix the IR-active modes that have a non-vanishing longitudinal component of the polarization thereby generating longitudinal IR-active modes (LO). This results in a splitting of the LO and TO frequencies for vanishing q vector that, in general, depends upon the direction (as noted in the angular dispersions of figure 2).

The angular dispersions of the LO modes have been already displayed in Figure V. For a more detailed discussion, and to assist in the interpretation of the figure, the frequencies of all the TO and LO modes of the three

relaxed supercells are given in Table VII with their symmetry labels and mode effective charges. For the (001) and (110) superlattices the LO frequencies are direction dependent and we give their values for \hat{q} parallel and perpendicular to the direction of compositional modulation in each supercell, corresponding to $\theta = 0$ and $\theta = 90$ deg in the angular dispersion shown in Figure 1, respectively. For the cubic (111) superlattice, symmetry considerations show that the LO frequencies do not depend upon \hat{q} .

Examination of the table shows that the (001) and (110) superlattices have unstable LO modes, a feature not present in the pure compounds. These modes are not confined, showing significant relative motion of the cations and anions in both the Zr and Ti centered subcells of the supercell. However, the induced polarizations in the two subcells are opposite in direction, and resulting near cancellation makes the unstable LO mode effective charges much smaller than those associated with the TO instabilities.

IV. DISCUSSION

As for the pure endpoint compounds, the unstable TO phonons are expected to be valuable indications of the existence and nature of a ferroelectric ground state for the PZT superlattices here considered, as they generate energy-lowering distortions with nonzero spontaneous polarization P_s under conditions of zero macroscopic electric field ($\mathbf{E} = 0$).

With dominant TO instabilities, PZT(001) and PZT(110) are virtually guaranteed to have ferroelectric ground states. In previous first-principles studies, attention has focused on ferroelectric structures of PZT(001) with polarization along the [001] direction. The two-mode behavior discussed here suggests that the true ground state could be both more complicated and more interesting. Freezing in the unstable TO phonons of the (001) superlattice give rise to a macroscopic polarization that is parallel to the interfaces in the PT layers for $\Gamma_{5'}$ and perpendicular to the interfaces in the PZ layers for $\Gamma_{1'}$. Depending on the anharmonic coupling between these modes and their coupling to homogeneous strain, either or both of these modes could freeze in to give a ground state structure with polarization along the [001] direction (the *c* phase), along [100] (the *a* phase), along [110] (the *aa* phase), in the (010) plane (the *ac* phase), or in the (110) plane (the designations of the phases correspond to those used in Ref. 30 in a different context).

The choice of equilibrium structure type from the list above should also be quite sensitive to the mechanical and electrical boundary conditions. Applied stresses, epitaxial constraints and applied electric fields will result in relative shifts of the two modes and changes in their coupling, and could result in transitions from one phase to another. In particular, this system might provide a

microscopic realization of a large-strain electrostrictive actuator as recently suggested by Bhattacharya.³¹

In contrast, PZT(111) has a dominant nonpolar instability, with the ferroelectric TO mode slightly higher in frequency. The ground state has been analyzed in detail by Fornari and Singh¹⁶. They observe, consistent with our results, that the ferroelectric and rotational distortions are quite competitive in energy and that this competition is very sensitive to strain.

The (001) and (110) supercells display LO as well as TO instabilities, a feature not present in the pure compounds. This presents the interesting possibility of a perpendicularly polarized ferroelectric ground state structure for a freestanding PZT film or nanoparticle. The energy of such a structure, with a depolarizing field $\mathbf{E} = -4\pi\mathbf{P}$, would in general be prohibitively high, corresponding to the stiffness of the LO mode. However, with an unstable LO mode, there would be a net energy gain despite the depolarizing field. Since Z^* is rather low for these modes, the spontaneous polarization would presumably be quite small, though still possibly observable or even useful. Whether this instability can be made to yield an actual ground state through application of appropriate mechanical boundary conditions remains to be investigated.

Aside from the physical implications of the calculated phonons, these results can also be used as a test of approximate schemes for obtaining the phonons of these and larger ordered superstructures. It is clear that while the virtual crystal approximation has been seen to work well for PZT(111), the requisite one-mode behavior of this structure is actually quite atypical. Generalizing from the lower symmetry PZT(001) and (110) structures, we expect that larger superstructures, with even lower symmetry, will exhibit multi-mode behavior. A key ingredient in reproducing this behavior is that approximations should allow for force constants involving Ti displacements to be different from the analogous force constants involving Zr displacements. The development and application of a suitable method, which was proposed in Ref. 5, will be the subject of a future publication.³²

V. SUMMARY

We have presented an ab initio study of the lattice dynamics of the high-symmetry nonpolar reference structures of three ordered configurations of PZT: the three ultrathin PT/PZ [1:1] superlattices (001), (110) and (111). In particular we focused on the zone-center lattice instabilities that can generate symmetry-breaking energy-lowering distortions and eventually lead to a phase transition. In PZT(001) and (110), these show a two-mode behavior that may have interesting consequences for ferroelectricity in these systems. Some direct connections between features of the superlattice structure and the unstable modes emerge. In general, if pure Ti-O chains

are present in the ordered structure, the lowest frequency unstable modes are confined in the PT layer and are characterized by displacements parallel to these chains. Another connection is between modes of the superlattice structures and those of strained bulk PT and PZ. Finally, we have verified that the character of the modes is not simply due to the small difference between the atomic mass of the intermixing cations, Ti and Zr, as is the case in some semiconductors, such as (Al,Ga)As, but that the effects of compositional modulation on the IFCs play an important role. Consequently, simple approximations for the IFC that neglect the effects of alloying, such as the virtual crystal approximation cannot provide an accurate description of the lattice dynamics in these systems.

ACKNOWLEDGMENTS

This work was supported by ONR N00014-00-1-0261. The work of K.M.R. was performed in part at the Aspen Center for Physics. The majority of the computations were performed at the Maui High Performance Computing Center.

-
- ¹ M. E. Lines and A. M. Glass, *Principles and Applications of Ferroelectrics and Related Materials* (Clarendon Press, Oxford, 1977).
 - ² N. E. Zein, Sov. Phys. Solid State **26**, 1825 (1984).
 - ³ S. Baroni, P. Giannozzi and A. Testa, Phys. Rev. Lett. **58**, 1861 (1987).
 - ⁴ Ph. Ghosez, J.-P. Michenaud and X. Gonze, Phys. Rev. **B58**, 6224 (1998).
 - ⁵ Ph. Ghosez, E. Cockayne, U. V. Waghmare and K. M. Rabe, Phys. Rev. B **60**, 836 (1999).
 - ⁶ C. LaSota, C.-Z. Wang, R. Yu and H. Krakauer, Ferroelectrics **194**, 109 (1997).
 - ⁷ R. Yu and H. Krakauer, Phys. Rev. Lett. **74**, 4067 (1995).
 - ⁸ B. Jaffe, R. S. Roth and S. Marzullo, J. Res. Nat. Bur. Stand. **55**, 239 (1955).
 - ⁹ V. K. Varadan, D. K. Ghodgaonkar, V. V. Varadan, J. F. Kelly and P. Glikerdas, Microwave J. **35**, 116 (1992).
 - ¹⁰ S. E. Park and T. R. Shrout, J. Appl. Phys. **82**, 1804 (1997).
 - ¹¹ H. Tabata, H. Tanaka and T. Kawai, Appl. Phys. Lett. **65**, 1970 (1994); E. D. Specht, H. M. Christen, D. P. Norton and L. A. Boatner, Phys. Rev. Lett. **80**, 4317 (1998).
 - ¹² G. Sághi-Szabó, R.E. Cohen, and H. Krakauer, Phys. Rev. B **59**, 12 771 (1999).
 - ¹³ L. Bellaiche and D. Vanderbilt, Phys. Rev. Lett. **83**, 1347, (1999).
 - ¹⁴ L. Bellaiche and D. Vanderbilt, Phys. Rev. B **61**, 7877 (2000).
 - ¹⁵ N.J. Ramer and A.M. Rappe, Phys. Rev. B **62**, R743 (2000).

- ¹⁶ M. Fornari and D.J. Singh, Phys. Rev. B **63**, 092101 (2001).
- ¹⁷ S. Baroni, S. de Gironcoli, A. Dal Corso, and P. Giannozzi, Rev. Mod. Phys. **73**, 515 (2001).
- ¹⁸ A. Dal Corso, A. Pasquarello, and A. Baldereschi, Phys. Rev. B **56**, 11 369 (1997).
- ¹⁹ S. Baroni, S. de Gironcoli, A. Dal Corso, and P. Giannozzi, <http://www.sissa.it/cm/PWcodes>
- ²⁰ D. Vanderbilt, Phys. Rev. B **41**, 7892 (1990).
- ²¹ D. M. Ceperley and B. J. Alder, Phys. Rev. Lett. **45**, 566 (1980); J. P. Perdew and A. Zunger, Phys. Rev. B **23**, 5048 (1981).
- ²² R. D. King-Smith and D. Vanderbilt Phys. Rev. B **49**, 5828 (1994).
- ²³ N. Troullier and J. L. Martins, Phys. Rev. B **43**, 1993 (1991).
- ²⁴ M. Born and K. Huang, *Dynamical Theory of Crystal Lattices* (Oxford University Press, Oxford, 1954).
- ²⁵ W. Cochran and R. R. Cowley, J. Chem. Phys. Solids **23**, 447 (1962).
- ²⁶ W. Zhong, R. D. King-Smith, and D. Vanderbilt, Phys. Rev. Lett. **72**, 3618 (1994).
- ²⁷ F. Bassani and G. Pastori Parravicini, *Electronic States and Optical Transitions in Solids* (Pergamon, Oxford, 1975), pp. 11-12.
- ²⁸ S. Baroni, P. Giannozzi, and E. Molinari, Phys. Rev B **41**, 3870 (1990).
- ²⁹ E. Molinari, S. Baroni, P. Giannozzi, and S. de Gironcoli, Phys. Rev B **45**, 4280 (1992).
- ³⁰ N. A. Pertsev, A. G. Zembilgotov and A. K. Tagantsev, Phys. Rev. Lett. **80**, 1988 (1998).
- ³¹ E. Burscu, G. Ravichandra and K. Bhattacharya, Appl. Phys. Lett. **77**, 1698 (2000).
- ³² C. Bungaro and K. M. Rabe, unpublished.

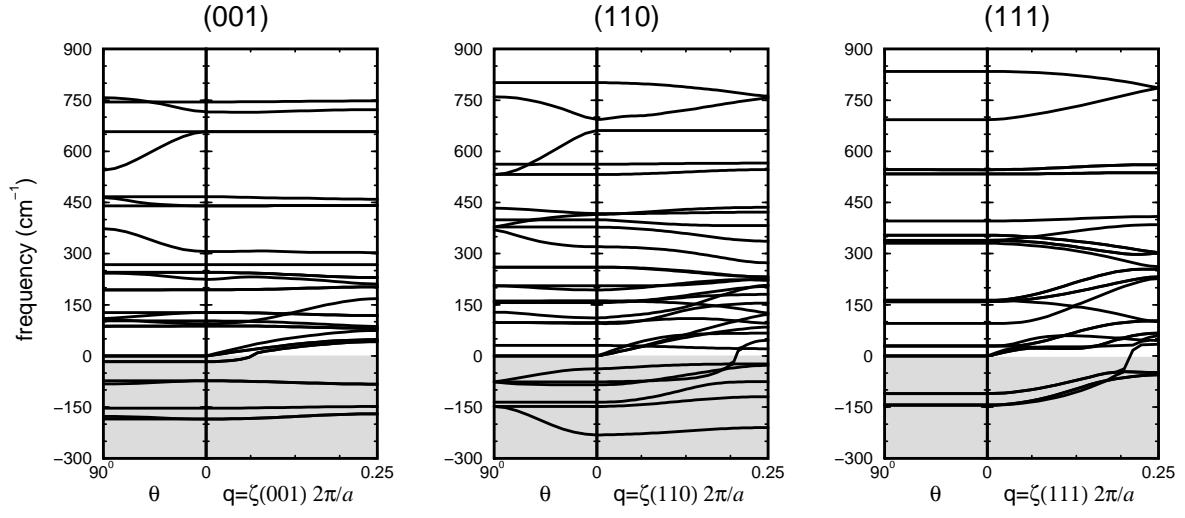


FIG. 1. Phonon dispersion along the direction of compositional modulation and $q=0$ anisotropy for the three relaxed PZT superlattice structures.

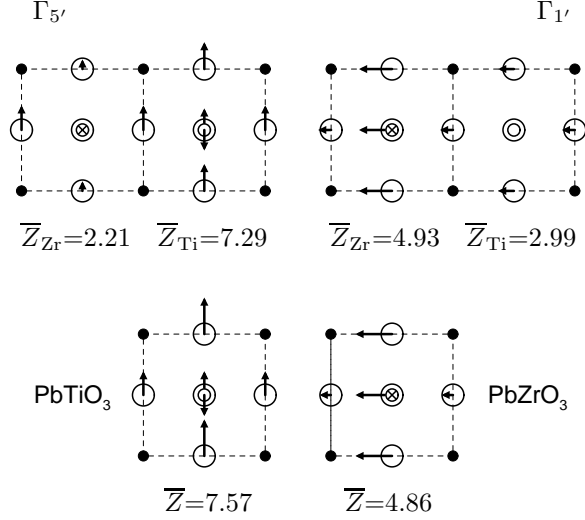


FIG. 2. Atomic displacements for the two most unstable TO polar modes in PZT(001), Γ'_5 and $\Gamma'_{1'}$, and the TO1 unstable modes of bulk PbTiO₃ and PbZrO₃. The projection in the (100) plane is shown. The different atomic species are represented as follows: small black circles for Pb, large white circles for O, small white circles for Ti, and small white circles with a cross for Zr. Note that the Zr displacement is close to zero in all modes shown and the atomic vibration in the Zr-centered cell is dominated by the displacements of the oxygen atoms.

TABLE I. Wyckoff labels and atomic positions, in reduced coordinates, for the three superlattice structures. For the (111) superlattice structure, the reduced coordinates are in terms of the lattice vectors of the conventional fcc unit cell. For Wyckoff positions with multiplicity greater than one, the first atom in the list will be referred to as the “representative atom.”

PZT (001)	Pb(2h)	(0.5 0.5 $\pm z_{\text{Pb}}$)
	Ti(1a)	(0 0 0)
	Zr(1b)	(0 0 0.5)
	O(2g)	(0 0 $\pm z_{\text{O}}$)
	O(2f)	(0 0.5 0), (0.5 0 0)
	O(2e)	(0 0.5 0.5), (0.5 0 0.5)
PZT (110)	Pb(2e)	(0.5 0 0.5), (0.5 0 0.5)
	Ti(1a)	(0 0 0)
	Zr(1c)	(0.5 0.5 0)
	O(4j)	($\pm x$ $\pm x$ 0)
	O(1b)	(0 0 0.5)
	O(1d)	(0.5 0.5 0.5)
PZT (111)	Pb(2c)	$\pm(0.25$ 0.25 0.25)
	Ti(1a)	(0 0 0)
	Zr(1b)	(0.5 0.5 0.5)
	O(6e)	($\pm x$ 0 0), (0 $\pm x$ 0), (0 0 $\pm x$)

TABLE II. Electronic dielectric tensor and Born effective charge tensors for representative atoms of the relaxed PZT(001) structure. Only the diagonal elements are given; the off-diagonal elements are zero by symmetry. The dielectric and Born effective charge tensors obtained by averaging the tensors computed for pure PT and pure PZ (at the average lattice parameter $a(\text{PZT})$) are given on the right hand side for comparison.

PZT(001)				average		
Pb	3.91	3.91	3.87	3.90	3.90	3.90
Ti	6.51	6.51	6.36	6.47	6.47	6.47
Zr	6.33	6.33	6.40	6.47	6.47	6.47
O(2g)	-2.54	-2.54	-5.20	-2.54	-2.54	-5.29
O(2f)	-2.77	-5.33	-2.28	-2.54	-5.29	-2.54
O(2e)	-2.36	-5.12	-2.78	-2.54	-5.29	-2.54
ϵ_{∞}	7.31	7.31	7.30	7.61	7.61	7.61

TABLE III. Electronic dielectric tensor and Born effective charge tensors for the relaxed PZT(110) structure. Only the diagonal elements are given, except for the O(4j) atoms; the off-diagonal elements are zero by symmetry. The dielectric tensor and Born effective charges obtained by averaging the tensors computed for pure PT and pure PZ (at the average lattice parameter $a(\text{PZT})$) are given on the right hand side for comparison. Note that in the (110) supercell the axis are rotated by 45 degrees around z with respect to the original cubic axes.

	PZT(110)			Average		
Pb	4.24	3.62	3.93	3.90	3.90	3.90
Ti	6.47	6.47	6.80	6.47	6.47	6.47
Zr	6.47	6.47	6.24	6.47	6.47	6.47
O(1b)	-2.49	-2.49	-5.48	-2.54	-2.54	-5.29
O(1d)	-2.61	-2.61	-5.07	-2.54	-2.54	-5.29
O(4j)	$\begin{pmatrix} -3.90 & -1.36 & 0 \\ -1.36 & -3.90 & 0 \\ 0 & 0 & -2.58 \end{pmatrix}$			$\begin{pmatrix} -3.92 & -1.38 & 0 \\ -1.38 & -3.92 & 0 \\ 0 & 0 & -2.54 \end{pmatrix}$		
ϵ_∞	7.31	7.31	7.41	7.61	7.61	7.61

TABLE IV. Frequencies and symmetry labels of the unstable eigenmodes of $D^T(q=0)$ for the relaxed and ideal PZT(001), (110) and (111) structures. The values in bold-faced type correspond to IR-active TO modes, the others being nonpolar modes. In PZT(001) and PZT(110) the corresponding atomic displacements are either parallel (\parallel) or perpendicular (\perp) to the direction of compositional modulation, as indicated. Frequencies are in cm^{-1} .

(001)		(110)		(111)	
relaxed	ideal	relaxed	ideal	relaxed	ideal
$\Gamma_{5'} \perp$	-185	-235	$\Gamma_{1'} \perp$	-231	-240
$\Gamma_{1'} \parallel$	-177	-151	$\Gamma_{5'} \parallel$	-148	-158
$\Gamma_{3'} \parallel$	-153	-72	$\Gamma_2 \parallel$	-134	-147
$\Gamma_{5'} \perp$	-73	-114	$\Gamma_{5'} \parallel$	-76	-71
$\Gamma_5 \perp$	-17	-22	$\Gamma_{1'} \perp$	-37	-67

TABLE V. The mode effective charge tensors, $\bar{\mathbf{Z}}$, associated with the unstable IR-active TO modes are decomposed into two contributions, one from the Zr-centered cell and one from the Ti-centered cell: $\bar{\mathbf{Z}} = \bar{\mathbf{Z}}_{\text{Zr}} + \bar{\mathbf{Z}}_{\text{Ti}}$. Results are shown for the relaxed and ideal PZT(001), (110) and (111) structures. The mode effective charges for the unstable TO modes of bulk PbZrO_3 and PbTiO_3 are given for comparison, both at the equilibrium volume and strained to the average volume of the 50% alloy, $V = a^3(\text{PZT})$.

superlattice			relaxed		ideal	
			$\bar{\mathbf{Z}}_{\text{Zr}}$	$\bar{\mathbf{Z}}_{\text{Ti}}$	$\bar{\mathbf{Z}}_{\text{Zr}}$	$\bar{\mathbf{Z}}_{\text{Ti}}$
(001)	$\Gamma_{5'} (\perp)$		2.21	7.29	1.57	8.11
	$\Gamma_{1'} (\parallel)$		4.93	2.99	4.44	3.71
	$\Gamma_{5'} (\perp)$		3.38	-1.56	3.76	-0.65
(110)	$\Gamma_{1'} (\perp)$		2.26	7.73	2.19	7.87
	$\Gamma_{5'} (\parallel)$		4.38	2.81	4.11	2.91
	$\Gamma_{5'} (\parallel)$		0.13	3.03	0.60	3.42
	$\Gamma_{1'} (\perp)$		2.74	0.04	3.10	-0.06
(111)	Γ_{15}		3.81	3.81	3.71	4.00
bulk			equilibrium		strained	
PbZrO_3			4.86		4.87	
PbTiO_3			7.57		8.00	

TABLE VI. The frequencies and local effective charges obtained for the relaxed superlattice structures when the Ti and Zr atoms are assumed to have the same atomic mass: $M_{\text{Ti}} = M_{\text{Zr}} = (M_{\text{Ti}} + M_{\text{Zr}})/2$.

superlattice			$\bar{\mathbf{Z}}_{\text{Zr}}$	$\bar{\mathbf{Z}}_{\text{Ti}}$	$\omega(\text{cm}^{-1})$
(001)	$\Gamma_{5'} (\perp)$		2.32	6.76	-177
	$\Gamma_{1'} (\parallel)$		4.98	2.99	-178
	$\Gamma_{5'} (\perp)$		3.36	-1.68	-70
(110)	$\Gamma_{1'} (\perp)$		2.42	7.12	-214
	$\Gamma_{5'} (\parallel)$		4.39	2.80	-148
	$\Gamma_{5'} (\parallel)$		0.11	3.02	-76
	$\Gamma_{1'} (\perp)$		2.82	0.00	-35
(111)	Γ_{15}		3.80	3.82	-110

TABLE VII. Frequencies and symmetry labels of the TO and LO zone-center eigenmodes. For PZT(001) and PZT(110) the LO frequencies are given for the two directions $\hat{\mathbf{q}}_{\perp}$ and $\hat{\mathbf{q}}_{\parallel}$ that are, respectively, perpendicular and parallel to the direction of compositional modulation. For PZT(111), the LO frequencies are independent of the direction of \mathbf{q} . For all modes, the mode effective charges are given in parentheses.

(001)				(110)				(111)				
TO		LO [$\hat{\mathbf{q}}_{\perp}$]	LO [$\hat{\mathbf{q}}_{\parallel}$]	TO		LO [$\hat{\mathbf{q}}_{\perp}$]	LO [$\hat{\mathbf{q}}_{\parallel}$]	TO		LO		
$\Gamma_{5'}$	-185 (9.50)	-82 (0.32)	94 (1.12)	$\Gamma_{1'}$	-231 (9.99)	-76 (1.16)	-85 (0.39)	Γ_{15}	-110 (7.62)	95 (1.34)		
$\Gamma_{1'}$	-177 (7.92)			$\Gamma_{5'}$	-148 (7.19)			Γ_{15}	159 (9.27)	330 (3.32)		
$\Gamma_{5'}$	-73 (1.82)	86 (0.25)	225 (1.73)	$\Gamma_{5'}$	-76 (3.16)		95 (0.72)	Γ_{15}	354 (3.27)	396 (4.23)		
$\Gamma_{5'}$	88 (0.59)	108 (0.95)		$\Gamma_{1'}$	-37 (2.78)	128 (2.11)	112 (1.00)	Γ_{15}	534 (5.65)	693 (9.90)		
$\Gamma_{1'}$	110 (3.53)			$\Gamma_{5'}$	98 (0.68)			194 (0.54)				
$\Gamma_{5'}$	127 (4.03)	193 (0.22)		$\Gamma_{5'}$	161 (4.00)							
$\Gamma_{5'}$	194 (0.62)	373 (5.31)	306 (4.72)	$\Gamma_{1'}$	161 (4.78)	370 (5.49)	320 (3.83)					
$\Gamma_{1'}$	243 (1.83)			$\Gamma_{5'}$	206 (2.96)			415 (3.53)				
$\Gamma_{5'}$	440 (1.73)	466 (3.80)		$\Gamma_{5'}$	378 (4.18)							
$\Gamma_{1'}$	465 (1.48)		467 (0.72)	$\Gamma_{1'}$	417 (1.12)	434 (3.54)	693 (9.94)					
$\Gamma_{1'}$	545 (6.86)		716 (10.11)	$\Gamma_{5'}$	532 (5.69)							
$\Gamma_{5'}$	658 (5.23)	757 (8.56)		$\Gamma_{1'}$	661 (5.35)	760 (8.49)						